Coded Aperture Compressive X-ray Spectral CT

Angela P. Cuadros, *Student Member, IEEE* and Gonzalo R. Arce, *Fellow, IEEE*Department of Electrical and Computer Engineering

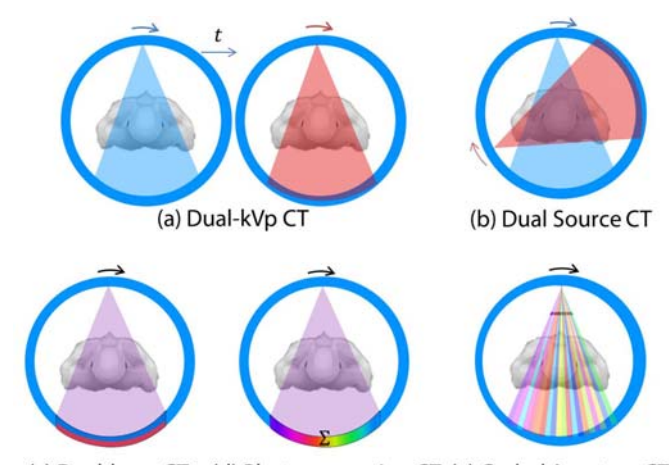
University of Delaware

Newark, DE 19716, USA

Abstract—Spectral computed tomography (SCT) makes use of the spectral dependence of X-ray attenuation in tissues and contrast agents to separate the attenuation data into more than two energy bins. Current SCT detectors are costly and the measured data have low signal to noise ratio due to the detector's narrow bin bandwidth and quantum noise. A new approach called coded aperture compressive X-ray SCT that combines a conventional rotating X-ray CT system with a set of pixelated K-edge coded apertures is introduced. In this method, the amplitude and spectra of the X-ray source are filtered by a particular pattern of K-edge filters in each view angle. Compressed sensing (CS) reconstruction algorithms are then used to recover the spectral CT image from the coded measurements. Simulations results for random coded apertures are shown, and their performance is compared to the use of uncoded measurements.

Index Terms—Spectral CT, coded apertures, image reconstruction, X-ray Imaging, K-edge imaging.

X-ray computed tomography (CT) has become essential in medical diagnosis. Tomographic gray scale images obtained from conventional systems, however, are often insufficient to reveal differences between materials having different chemical composition but the same X-ray attenuation coefficient. Spectral Computed Tomography (SCT) not only provides morphological information, as conventional CT scans do, but it also allows material decomposition as well [1]. Thus, the emerging field of SCT has important applications in medical imaging and transit security. Among the current spectral data acquisition approaches are dual-energy CT, which makes use of two sequential CT scans with different X-ray tube voltages or a dual source X-ray CT system (Figs. 1(a,b) respectively), or a set of sandwiched detectors, to obtain two datasets with distinct attenuation characteristics (Fig. 1(c)). The latter approach is widely used in luggage security inspection due to its temporal and spatial resolution, material identification ability and low-cost [2]. On the other hand, higher energy resolution can be achieved by using photon counting detectors (PCDs, Figs. 1(d)), which can identify the energy of incoming photons and record the data in the corresponding energy bins [3]. The advantages of spectral tomography, however, are hindered by several technical challenges that prevent their broad practical application including costly photon counting detectors and their low signal to noise ratio [4]. Conventional X-ray detectors can also be used if these are equipped with heavy K-edge filters which are switched in sequential monoenergetic X-ray flux measurements [5]. A K-edge filter is a material consisting of a high-Z element (elements with a high atomic number), such as tantalum, tungsten or molybdenum which sharply cuts off part of the X-ray spectrum above the



(c) Dual-layer CT (d) Photon counting CT (e) Coded Aperture CT

Fig. 1: Spectral CT detector modalities. Dual Energy: (a) dual sequential scanning (dual energy); (b) Dual-source scanning;(c) Sandwich layered detector. Multi-Spectral Energy: (d) Photon counting detector; (e) K-Edge coded aperture.

element's K-shell electrons' binding energy (K-edge). However, this technique requires multiple scans, often preventing their practical implementation.

This paper explores a radical departure from conventional methods used in SCT. It relies on X-ray coded projections to circumvent many of the above-mentioned limitations. Rather than measuring objects by the attenuated X-rays, the Xrays are first coded in amplitude and spectra by blocking or unblocking a known pattern, effectively creating a coded aperture on the path of the X-ray measurements (Fig. 1(e)). The coded apertures, create lower-dose structured X-ray bundles that interrogate specific pixels of the object. Structured illumination, can also be used to reduce the number of angles by source multiplexing in limited angle geometries. The coded aperture elements are chosen to be K-edge filter materials in order to obtain multiplexed energy-binned sinograms. The resulting ill-posed problem is solved using compressed sensing reconstruction algorithms to recover the energy-binned CT images.

The remainder of this paper is organized as follows: Section II describes the forward model of the proposed SCT systems. The simulation results are presented in Section III. Finally, Section IV presents the conclusions and future work.

I. FORWARD PROJECTION MODEL

Spectral/polychromatic X-ray tomography is based on the Beer-Lambert law for polychromatic X-rays [6], given by

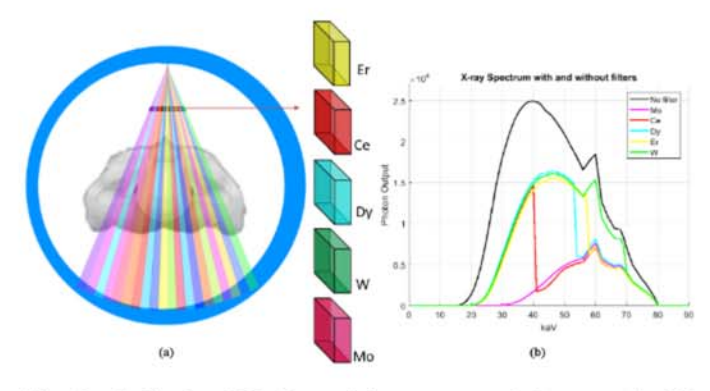


Fig. 2: (a) Pixelated K-edge coded aperture mask for a rotating X-ray imaging system. (b) Filtered spectra of an 80 keV X-ray source when using Mo, Ce, Dy, W and Mo as filters

 $I(E) = I_0(E)e^{-\int_{\ell(y)}\mu(y,E)dy}$, where $\mu(y,E)$ is the energydependent linear attenuation coefficient in a spatial position y along an X-ray beam path $\ell(y)$, and $I_0(E)$ is the initial photon count at the energy E. For photon counting detectors with multiple energy bins, a measurement in an energy bin E_k can be approximately described by the mono-energetic Beer-Lambert law: $I = I_0 \cdot e^{-\int_0^\infty \mu(x) dx}$, where I_0 is the intensity of the X-ray beam, I is the measured intensity and $\mu(x)$ is the linear attenuation coefficient. The imaging model needs to be discretized since only a discrete number of measurements can be taken. Thus, for each energy bin E_k , the photon count \mathbf{y}_k is given by the linear equation $\mathbf{y}_k = \mathbf{W}\mathbf{x}_k$, where $\mathbf{x}_k \in \mathbb{R}^{N^2}$, represents the effective attenuation coefficients of a $N \times N$ discretized object at energy E_k and W is the system matrix, where each of the elements in $\mathbf{W} \in \mathbb{R}^{MP \times N^2}$ represents the intersection length of each ray with every pixel inside the image, with a row index corresponding to a line integral and column index corresponding to an image pixel, M corresponds to the number of detectors per view angle, and P is the number of view angles. Note the matrix W is the same for all K energies.

The reconstruction of the K images, for each energy level, can be solved independently, using the total variation (TV) regularization algorithm, as in [7]. However, this approach does not take into account the highly correlated data across energies. Furthermore, photon counting detectors are prohibitively costly for some applications and present difficulties to balance the number of energy bins and the statistical noise in each bin [8]. Thus, alternative systems to obtain energy binned sinograms is a research topic of broad interest [9]. Spectral CT using conventional X-ray detectors with multiple balanced K-edge filters (Ross filters) was proposed by Rakvongthai et al. in [5]. The thickness values of the filters are such that the transmitted spectra through any two filters are nearly identical except in the energy band between their respective Kedges. In this architecture, five balanced K-edge filters are used separately in conjunction with an existing CT system with energy integrating detectors to obtain synthesized energy-binned attenuation images using filtered back projection (FBP). In principle, Ross filters are to be carefully matched in thickness; however, measurement modeling can be used to obtain quasi-

monoenergetic intensity for energy bins. Thus, the measured filtered sinograms are a linear combination of the energybinned sinograms defined by the K-edge energies of the used filters. This can be written as $y_{i,\ell} = \sum_{k=1}^K b_{i,\ell}^k y_{i,k}$, where $y_{i,\ell}$ is the intensity measured by the i^{th} detector when the X-ray beam is filtered using the ℓ^{th} filter, for $\ell=1,\cdots,F$ with Fthe number of filters used; $y_{i,k}$ is the intensity corresponding to the k^{th} energy bin, for $k=1,\cdots,K$ where K is the number of energy bins. The value of the coefficients $b_{i,\ell}^k$ is computed as $b_{i,\ell}^k = ((E_k - E_{k-1}))^{-1} \int_{E_{k-1}}^{E_k} e^{-\mu_\ell(E)t_{i,\ell}/\cos(\theta_i)}$, where $\mu_{\ell}(E)$ is the attenuation coefficient for the ℓ^{th} filter with $t_{i,l}$ thickness and θ_i is the angle between the normal of the filter surface and the line connecting the source and the detector. Figure 2(b) illustrates the transmitted energy spectra of an 80 kVp X-ray source, seen through the five balanced filters used in this paper [Molybdenum (Mo), Cerium (Ce), Dysprosium (Dy), Erbium (Er), and Tungsten (W)]. The measurements obtained for each (Ross) filter are denoted by $\mathbf{y}^F = \mathbf{B}\mathbf{y}^E$, where $\mathbf{B} \in \mathbb{R}^{FMP \times KMP}$ is called the transmission matrix and contains the weights $b_{i,\ell}^k$ that relate the filtered sinograms (measured intensity, \mathbf{y}^F) with the energy-binned sinograms (quasi-monoenergetic intensity, \mathbf{y}^E). Rakvongthai uses the least squares (LS) solution to obtain the energy binned sinograms from the filtered sinograms as $\hat{\mathbf{y}}^E = \mathbf{B}^T (\mathbf{B}\mathbf{B}^T)^{-1} \mathbf{y}^F$. The linear attenuation coefficients of the $N \times N$ discretized object for the K energy bins $\mathbf{x} \in \mathbb{R}^{KN^2 \times 1}$ are then independently reconstructed from the energy binned sinograms using the FBP algorithm. This scheme overcomes the challenges of photon counting detectors, but the acquisition time is longer since different scans are needed for each filter material. Furthermore if used in a clinical application the radiation dose is increased. We propose a different approach to sense the spectral tomography pixels and to reconstruct the energy resolved image stacks. Our approach is based on the use of pixelated Kedge coded apertures to obtain spatially and spectrally coded illumination projections of the object. The pixels of the coded apertures are composed by balanced filters (Ross filters), that consist of materials with nearly adjacent atomic numbers such that the transmitted spectra through the filters differ in the energy band between their respective K-edges [10]. Figure 2 depicts the pixelated K-edge coded aperture X-ray imaging system and the filtered spectra for a mask using a particular set of Ross filters. When coded apertures are introduced in the system, and the coded aperture elements have a one to one correspondence with the detector elements, a particular filter element modulates the X-ray intensity measured in each detector. Thus, the measurements correspond to a spectrally coded sinogram that multiplexes the filtered measurements (see Fig. 3(b)). Note that each measurement has a different color intensity corresponding to the filter used for that particular X-ray beam. Mathematically, let $\mathbf{C} \in \mathbb{R}^{MP \times FMP}$ be the coding matrix accounting for the coded apertures where the coded aperture element $[\mathbf{C}]_{i,(\ell-1)MP+1}$ is 1 when the X-ray beam is filtered using the ℓ^{th} filter, 0 otherwise. Hence, the multiplexed measurements $\mathbf{y} \in \mathbb{R}^{MP}$ are given by $\mathbf{y} = \mathbf{C}\mathbf{y}^F$.

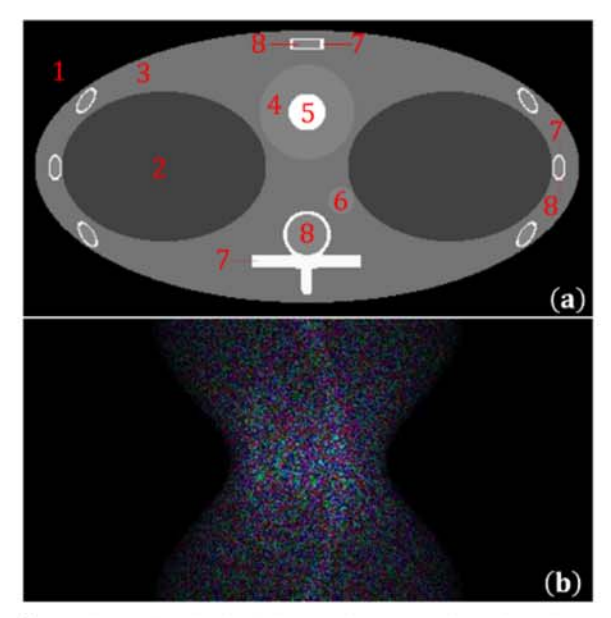


Fig. 3: (a) Simplified Forbild thorax phantom, where the sub-regions are defined in Table I. (b) Spectrally coded sinogram of the Forbild thorax phantom with multiplexed measurements using pixelated K-edge coded aperture projections.

In order to obtain the linear attenuation coefficients from the multiplexed measurements the inverse problem can be expanded as:

$$\mathbf{y} = \mathbf{C}\mathbf{B}\mathbf{y}^E = \mathbf{C}\mathbf{B}(\mathbf{I}_{K\times K}\otimes\mathbf{W})\mathbf{x} = \mathbf{H}\mathbf{x},$$
 (1)

where W contains the intersection length of each ray with each pixel inside the image, & denotes the Kronecker product and $\mathbf{I}_{K \times K} \in \mathbb{R}^{K \times K}$ is an identity matrix. Note that the Kronecker compressed sensing (KCS) model introduced by Duarte and Baraniuk in [11] has been used to describe the sensing of the energy dependent linear attenuation coefficients, given that the same measurement CT matrix W is applied to each energy band image. Furtheremore, a Kronecker product between a discrete Fourier transform (DCT) and a 2D Wavelet transform is used as a sparsifying transform for the energy and spatial domains respectively. When the sparsity properties of the object x in a basis Ψ are used, the problem can be rewritten as $y = H\psi\theta$, where $x=\Psi\theta$ and θ is a column vector whose entries are the coefficients representation in the basis. The recovery of θ is obtained as the solution to the nonlinear optimization problem [12]

$$\hat{\boldsymbol{\theta}} = \underset{\mathbf{z}}{\operatorname{argmin}} \ \frac{1}{2} ||\mathbf{A}\mathbf{z} - \mathbf{y}||_2^2 + \tau ||\mathbf{z}||_1, \tag{2}$$

where $\mathbf{A} = \mathbf{H} \mathbf{\Psi}$ is the sensing matrix of the problem and τ is a regularization parameter.

II. RESULTS

A simulation experiment for an X-ray parallel beam system with pixelated K-edge coded apertures is performed using a 256×256 modified Forbild thorax phantom [13]. The modified phantom consists of eight different materials to simulate lung, heart, artery, bone, soft tissue, air, iodine and marrow. Figure 3(a) shows this thorax phantom, with the tissues and materials defined in Table I.

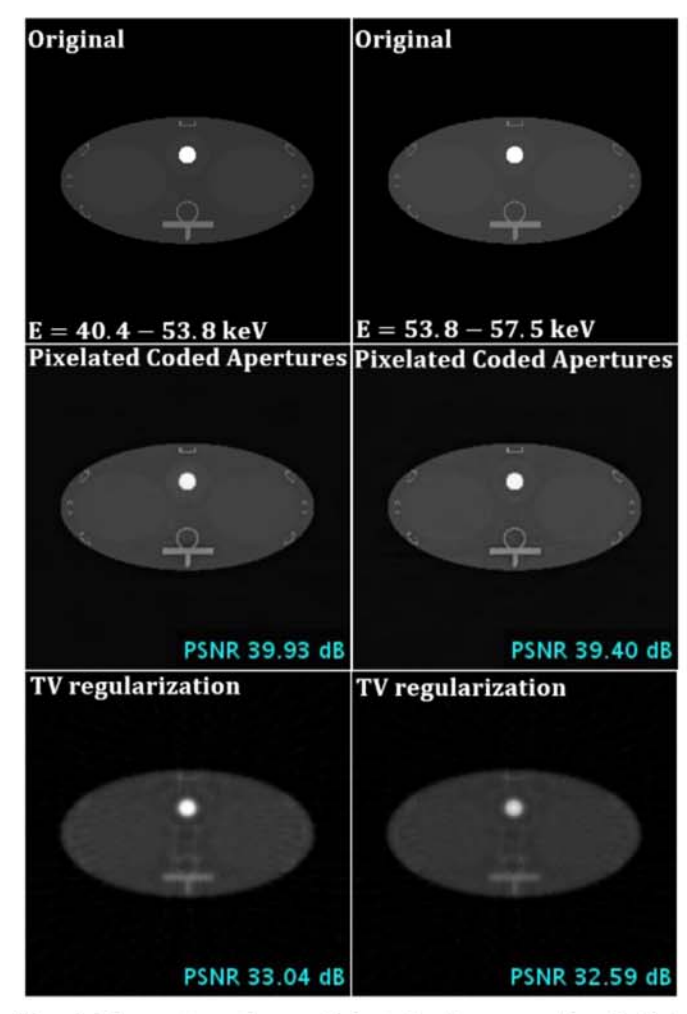


Fig. 4: Linear attenuation coefficients for the energy bins E=40.4-53.8 and E=53.8-57.5 keV. Reconstructions using random pixelated K-edge coded apertures and a TV regularization algorithm for a single channel with an equivalent amount of data (35 view angles)

TABLE I: Material types of the sub-regions in the modified Forbild thorax phantom

Number	Material	Density (g/cm ³)
1	Air	0.00
2	Lung	0.26
3	Average Soft Tissue	1.00
4	Heart (Blood)	1.06
5	ROI (0.9% Iodine + 99.1% Blood)	1.09
6	Artery (Blood)	1.06
7	Bone	1.50
8	Marrow	0.98

In this paper, the thicknesses for the filters were chosen as in [5]; that is, 8,6,3,3,1 mil (1 mil = $25.4 \mu m$) for the Mo, Ce, Dy, Er and W filters respectively. The energy bins defined by these K-edge filters are 20.0-40.4, 40.4-53.8, 53.8-57.5, and 57.5-69.5 keV. The X-ray spectrum was simulated at 80 kVp using the Spektr software and the system matrix W for a parallel beam X-ray system with 180 projection angles was obtained using the ASTRA tomography toolbox [14]. Using the spectrally coded sinogram measurements in Fig.3 (b), obtained using a random set of coded apertures

for each view angle, 4 energy-binned linear attenuation images are obtained by solving the minimization problem in (2) using a modified version of the gradient projection for sparse reconstruction (GPSR) algorithm. The modified GPSR includes a filtering step, as proposed by Mejia et al. in [15], which yields improved quality using fewer iterations. The energy binned CT image is represented on the basis $\Psi = \Psi_{DCT} \otimes \Psi_{2D-W}$ where Ψ_{DCT} is DCT basis for the energy domain and Ψ_{2D-W} is the 2D wavelet basis for the spatial domain. The information recovered from the 4 energy bins can be further combined to distinguish the 8 materials. Figure 4 shows the reconstruction for the third energy bin for random coded apertures, which has a Peak signal-to-noise ratio (PSNR) of 39.8 dB.

TABLE II: Material types of the sub-regions in the modified Forbild thorax phantom

Energy Bin	Random Codes (PSNR dB)	ASD-POCS (PSNR dB)
1	29.21	27.00
2	35.63	29.08
3	39.93	33.04
4	39.40	32.59

We compared our new SCT signal model and reconstructions with the ASD-POCS algorithm [7]. First, the measurements are subsampled to obtain a radiation dose equivalent to the dose used in the SCT model proposed in this paper. For the simulation parameters, this is equivalent to a parallel beam system with 35 projection angles and energy resolving detectors with energy bin widths of 20.0-40.4, 40.4-53.8, 53.8-57.5, and 57.5-69.5 keV. Images at individual energy bins were reconstructed independently using a TV-regularization algorithm, and as it can be seen in Fig. 4, for the third and fourth energy bins our system outperforms this approach by approximately 6 dB. Table II shows the PSNR for the 4 energy bins that can be reconstructed using the algorithm proposed in this paper and the comparison with the TV regularization algorithm in [7].

III. DISCUSSIONS AND CONCLUSION

The concept of an SCT system using conventional CT systems together with a set of pixelated K-edge coded aperture filters is proposed. The simulations showed that the reconstructed attenuation coefficients for different energy windows obtained using the proposed algorithm, outperform reconstructions using an equivalent radiation dose and photon counting detectors. The proposed SCT approach has the potential to provide a cost-effective alternative to photon counting spectral CT techniques and an optimized time solution for multiple Kedge filter scanning. The measurement model can be applied to different X-ray source geometries such as fan beam and X-ray tomosynthesis by modifying the matrices **B** and **W** accordingly. Additionally, the simulation of distinct sets of Ross filters to obtain different energy bins will be studied in future work as well as the formulation of an improved compressive coded aperture spectral model using a rank minimization constraint to solve the inverse problem.

In order to implement a testbed to experimentally validate the SCT system with pixelated K-edge coded apertures, the elements of the coded apertures will be modeled to take 2 values, 0 to filter the X-ray beam or 1 to let the X-ray beam pass. The coded aperture will be 3D printed in acrylic and modeled such that 0 corresponds to a hole in the acrylic plate. The mold is then filled with metal powders of the materials that constitute a set of balanced Ross filters in the corresponding positions. The thicknesses of the pixels in the coded apertures are fixed so that the transmitted X-ray energy spectra are almost identical except in the energy band between the K-edges of the set of Ross filters. For each rotation, a different pixelated K-edge coded aperture mask will be placed in front of the source to obtain the spectrally coded measurements and the inverse problem in (5) will be solved.

REFERENCES

- [1] I. Glass, A. P. H. Butler, P. H. Butler, P. J. Bones, and S. J. Weddell, "Physiological gating of the mars spectral micro ct scanner," in 2013 28th International Conference on Image and Vision Computing New Zealand (IVCNZ 2013), Nov 2013, pp. 317–322.
- [2] G. Zentai, "X-ray imaging for homeland security," in 2008 IEEE International Workshop on Imaging Systems and Techniques, Sept 2008, pp. 1–6.
- [3] Q. Yang, W. Cong, and Y. X. G. Wang, "Spectral x-ray ct image reconstruction with a combination of energy-integrating and photon-counting detectors," *PLOS ONE*, vol. 11, no. 5, pp. 1–15, 05 2016.
- [4] L. Li, Z. Chen, W. Cong, and G. Wang, "Spectral ct modeling and reconstruction with hybrid detectors in dynamic-threshold-based counting and integrating modes," *IEEE Transactions on Medical Imaging*, vol. 34, no. 3, pp. 716–728, March 2015.
- [5] Y. Rakvongthai, W. Worstell, G. E. Fakhri, J. Bian, A. Lorsakul, and J. Ouyang, "Spectral ct using multiple balanced k-edge filters," *IEEE Transactions on Medical Imaging*, vol. 34, no. 3, pp. 740–747, March 2015.
- [6] L. Li, Z. Chen, G. Wang, J. Chu, and H. Gao, "A tensor prism algorithm for multi-energy ct reconstruction and comparative studies," *Journal of X-Ray Science and Technology*, vol. 22, no. 2, pp. 147–163, 2014.
- [7] P. X. Sidky EY, "Image reconstruction in circular cone-beam computed tomography by constrained, total-variation minimization," in *Physics in medicine and biology*, 2008, pp. 4777–4807.
- [8] L. Li, Z. Chen, W. Cong, and G. Wang, "Spectral ct modeling and reconstruction with hybrid detectors in dynamic-threshold-based counting and integrating modes," *IEEE Transactions on Medical Imaging*, vol. 34, no. 3, pp. 716–728, March 2015.
- [9] G. Wang, A. Butler, H. Yu, and M. Campbell, "Guest editorial special issue on spectral ct," *IEEE Transactions on Medical Imaging*, vol. 34, no. 3, pp. 693–696, March 2015.
- [10] P. Ross, "Polarization of x-rays," Phys. Rev, vol. 28, pp. 425, 1926.
- [11] M. F. Duarte and R. G. Baraniuk, "Kronecker compressive sensing," IEEE Transactions on Image Processing, vol. 21, no. 2, pp. 494–504, Feb 2012.
- [12] M. A. Davenport, M. F. Duarte, Y. C. Eldar, and G. Kutyniok, "Introduction to compressed sensing," in *Compressed Sensing*, G. K. Yonina C. Eldar, Ed. Cambridge University Press, 2012.
- [13] A. Maier, H. G. Hofmann, M. Berger, P. Fischer, C. Schwemmer, H. Wu, K. Mller, J. Hornegger, J. H. Choi, C. Riess, A. Keil, and R. Fahrig, "Conrad-a software framework for cone-beam imaging in radiology," *Medical Physics*, vol. 40, no. 11, 2013.
- [14] W. Xu, F. Xu, M. Jones, B. Keszthelyi, J. Sedat, D. Agard, and K. Mueller, "High-performance iterative electron tomography reconstruction with long-object compensation using graphics processing units (gpus)," *Journal of structural biology*, 2010.
- [15] Y. Mejia and H. Arguello, "Filtered gradient reconstruction algorithm for compressive spectral imaging," *Optical Engineering*, vol. 56, no. 4, pp. 041306, 2016.